Inorganic Chemistry

Article

pubs.acs.org/IC

Intermolecular Binding Modes in a Novel [1 + 1] Condensation 1*H*-Pyrazole Azamacrocycle: A Solution and Solid State Study with Evidence for CO_2 Fixation

Raquel Belda,[†] Javier Pitarch-Jarque,[†] Conxa Soriano,[‡] José M. Llinares,[†,‡] Salvador Blasco,[†] Jesús Ferrando-Soria,[§] and Enrique García-España*[,†]

[†]Instituto de Ciencia Molecular, Universidad de Valencia, C/Catedrático José Beltrán Martínez, no. 2, 46980 Paterna, Valencia, Spain

[‡]Departamento de Química Orgánica, Facultad de Farmacia, Universidad de Valencia, Avda. Vicente Andrés Estellés s/n 46100, Burjassot Valencia, Spain

[§]Department of Chemistry, Texas A&M University, College Station, Texas 77843, United States

Supporting Information

ABSTRACT: The synthesis of a novel cyclophane (**L1**) consisting of a 1*H*-pyrazole moiety linked through methylene groups to a 1,5,9,13-tetraazadecane chain is described. As far as we know, this is one of the first reported syntheses of a [1 + 1] condensation 1*H*-pyrazole azamacrocyclic ligand. The crystal structures of the complexes $[Cu_2(H(H_{-1}\mathbf{L1}))(H_{-1}\mathbf{L1})](ClO_4)_3{\cdot}3.75H_2O$ (**1**) and $([Cu_2(H(H_{-1}\mathbf{L1}))_{0.5}(H_{-1}\mathbf{L1})_{1.5}]_2(ClO_4)_3Br_2{\cdot}4.2H_2O$ (**2**) show that Cu^{2+} coordination leads to formation of 2:2 Cu^{2+}:L dinuclear dimeric complexes in which the 1*H*-pyrazole units lose a proton behaving as bis(monodentate) bridging ligands. Unlike previously reported complexes of [2 + 2] pyrazole azamacrocycles, the pyrazolate units in **1** are pointing outward from the macrocyclic cavity to bind the Cu^{2+} ions. Inner coordination with formation of 1:1 Cu^{2+}:L complexes is however observed in [1 + 1] pyridine azamacrocycles as shown by the crystal structure here presented of the complex $[Cu\mathbf{L2}](ClO_4)_2$ (**3**). Crystals of $[Cu_3(H_{-1}\mathbf{L1})_2(CO_3)(H_2O)](ClO_4)_2{\cdot}8H_2O$ (**4**) grown by evaporating aqueous solution at pH 9 containing Cu^{2+} and **L1** in 3:2 molar ratio show the presence of a further Cu^{2+} coordinated to the two free amine groups found in structures **1** and **2**. The metal ion fills its coordination sphere capturing atmospheric CO_2 as a η^1,η^2-bidentate carbonate anion placed in the equatorial position and an axial water molecule. pH-metric data, UV−vis spectroscopic data, EPR measurements, and HR-ESI-MS data support that the outer coordination mode with formation of 2:2 dinuclear dimeric and 3:2 trinuclear complexes is preserved in aqueous solution.

INTRODUCTION

Organic compounds with 1*H*-pyrazole units have raised a great deal of interest in the past years due to the interesting hydrogen bonding and coordination properties of this small heterocycle.[1−3] Indeed, 1*H*-pyrazole in its neutral form can behave both as a hydrogen bond acceptor and donor, while in its pyrazolate anionic form it can accept two hydrogen bonds from appropriate donor groups. With respect to metal coordination, neutral 1*H*-pyrazole typically acts as a monodentate ligand while as a pyrazolate anion it behaves typically as a bridging bis(monodentate) or exobidentate ligand (Scheme 1).[1−4]

Many ligands have been built with a pyrazole unit spacing two either equivalent or different coordination sites with the idea of placing two interconnected metal ions in close proximity in order to explore their electronic and magnetic interactions (see Scheme 2).[3,5−8] Other spacers containing two adjacent nitrogen atoms able to provide similar organizations are piridazines,[9,10] 1,2,4,5-tetraazines,[11] 1,2,4-triazoles,[12−14] 1,3,4-thiadiazoles, and 1,3,4- oxadiazoles.[15] In recent years some of us have contributed to this topic with the preparation and study of the supramolecular and coordination chemistry of a series of azamacrocycles formed either by [2 + 2] or [3 + 2] condensation of 1*H*-pyrazole-3,5-dicarbaldehyde with different triamines or with the tripodal tetraamine tris(2-aminoethyl)-amine, respectively.[16−20] These studies evidenced interesting binding capabilities toward metal ions and organic molecules of biological relevance, such as amino acids or dopamine. With respect to metal ion coordination, the preferred coordination

Scheme 1. Coordination Modes of Pyrazole

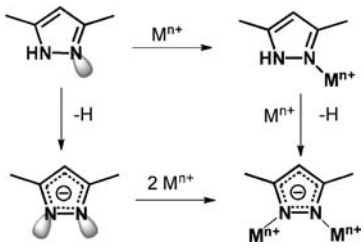

Received: March 15, 2013
Published: September 16, 2013

 © 2013 American Chemical Society

Scheme 2. Kinds of Polynuclear Complexes of Pyrazole Ligands

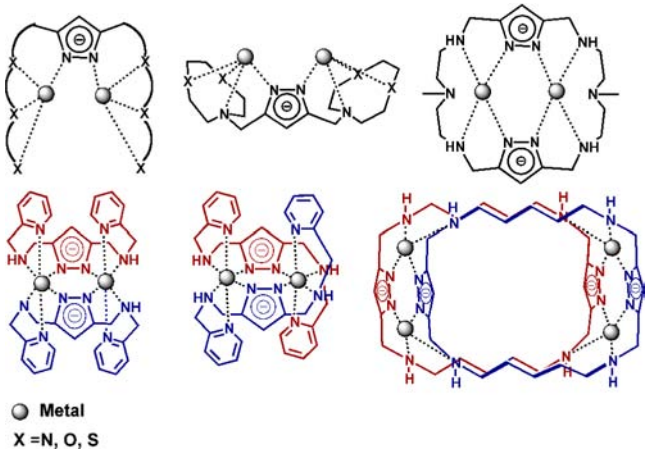

mode of pyrazole was as a bis(monodenate) pyrazolate anion bridging two metal ions in the interior of the macrocycle (Scheme 2).

However, in spite of all these interesting chemical features, as far as we know [1 + 1] pyrazole azamacrocycles had not yet been reported. This kind of macrocycle can give rise to novel binding modes due to the fact that an outer orientation of the pyrazole nitrogen atoms favors intermolecular organizations with the metal ion linking more than one ligand (Scheme 2). Moreover, these metal complexes might behave as receptors for additional metal ions which in their turn can bind other target substrates through the formation of mixed metal complexes. Such an outer orientation has been somehow evidenced by the tetranuclear macrocyclic cage formed when two 1*H*-pyrazole units are condensed with two 1,5-diazapentane (cadaverine) diamines in the presence of Cu^{2+} (Scheme 2).[21]

Here we report the synthesis of the first macrocycle of this [1 + 1] series (**L1**) (Chart 1). **L1** is made by linking the polyamine 1,5,9,13-tetraazatridecane through methylene groups to the 3,5-positions of a 1*H*-pyrazole ring.

Chart 1

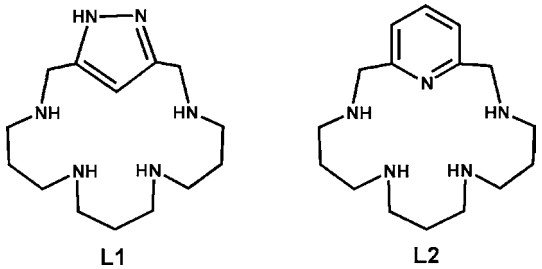

We have also studied the Cu^{2+} coordination of **L1**. Formation of mononuclear, binuclear complexes with 2:2 Cu^{2+}:**L1** stoichiometry and trinuclear ones with 3:2 Cu^{2+}:**L1** stoichiometry has been evidenced through different solution and solid state techniques. Furthermore, we show that the 3:2 Cu^{2+}:**L1** complexes are able to fix atmospheric carbon dioxide in water with remarkable affinity. For comparison, we have also studied the Cu^{2+} coordination chemistry of a related macrocycle (**L2**) containing a 2,6-dimethylpyridine linker connecting the ends of the same polyamine chain.[22]

RESULTS AND DISCUSSION

Synthetic Procedure. The synthesis of **L1** and **L2** was performed according to a modification of the well-known Richman−Atkins procedure,[23] which is based on a macrocyclation reaction of the tosylated polyamine with either 1*H*-3,5-bis(chloromethyl)pyrazole or with 2,6-bis(bromomethyl)-pyridine in CH_3CN using K_2CO_3 as a base. However, in the case of **L1**, to avoid side reactions, it was first necessary to protect the nucleophilic NH group of pyrazole by reaction with 3,4-dihydroxypyran in CH_2Cl_2.[24] 1*H*-3,5-Bis(chloromethyl)-pyrazole was prepared from 1*H*-3,5-pyrazoledicarboxylate in a three-step procedure which consists first of esterification in ethanol, followed by reduction with di(isobutyl)aluminum hydride (DIBAL) to obtain the diol and then treatment with thyonyl chloride (Scheme 3).[25] An alternative synthesis of the macrocycle **L2** had been previously reported by I. Dierk et al.[22]

Scheme 3. Synthesis of L1

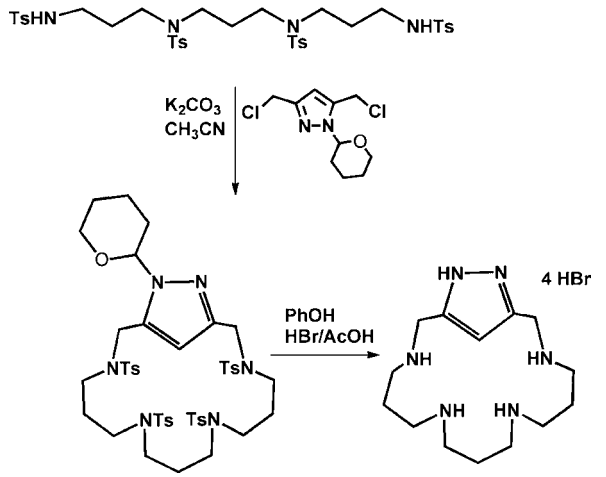

Acid−Base Properties. The basicity constants of **L1** and **L2** are shown in Table 1. Both ligands present four protonation steps in the pH range available for the potentiometric measurements (pH 2.5−11.0). Except for the first one, **L1** displays higher basicity than **L2** for all the protonation steps. Moreover, although the pyrazole or pyridine units may bear themselves an additional protonation step, we have not detected such a protonation constant. UV−vis spectra of **L1** recorded at variable pH do not show any significant change below pH 4 supporting that the pyrazole ring does not protonate in this pH range (see Supporting Information, Figure

Table 1. Logarithms of the Basicity Constants for Compounds L1 and L2 Determined in 0.15 M $NaClO_4$ at 298.1 K[a]

reaction[b]	L1	L2
L + H ⇆ HL	10.63(2)[c]	10.60(3)
HL + H ⇆ H_2L	9.35(1)	8.57(3)
H_2L + H ⇆ H_3L	7.24(2)	6.73(3)
H_3L + H ⇆ H_4L	5.58(2)	5.27(4)
log β	32.80(3)	31.17(5)

[a]Logarithms of the stepwise (K_{H_iL}) and cumulative [β = (ΠK_{H_iL})] protonation constants are reported. [b]Charges omitted. [c]Values in parentheses are standard deviations in the last significant figure.

dx.doi.org/10.1021/ic400645t | Inorg. Chem. 2013, 52, 10795−10803

S1). However, a plot of the absorbance at 225 nm overlapped with the species distribution diagram (Figure 1a) denotes that

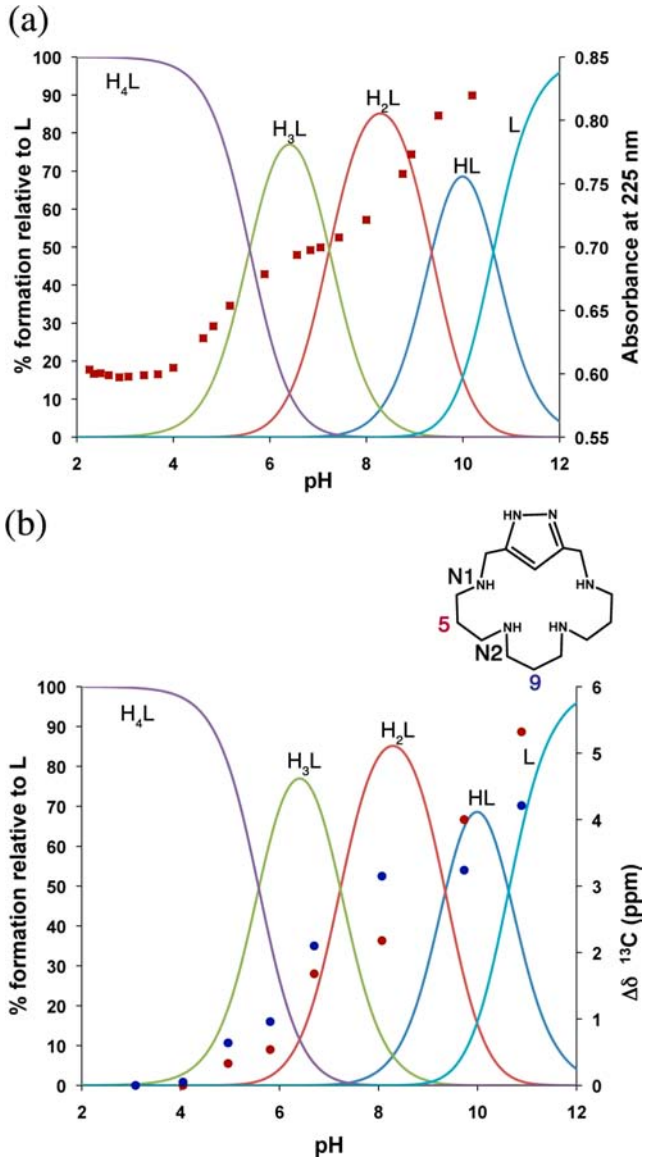

Figure 1. Plot of the species distribution diagram of **L1** along with (a) the variation in the absorption at 225 nm with pH (pH values 2.26, 2.35, 2.49, 2.66, 2.88, 3.07, 3.39, 3.68, 4.00, 4.62, 4.83, 5.17, 5.89, 6.56, 6.84, 7.05, 7.43, 8.00, 8.75, 8.93, 9.49, and 10.19) and (b) variations with pH of the chemical shifts of ^{13}C NMR signals of C5 (red) and C9 (blue) (pH values 3.09, 4.05, 4.96, 5.81, 6.70, 8.07, 9.73, and 10.89).

significant changes occur following the second and fourth protonation steps (H_2L1^{2+} and H_4L1^{4+} species, respectively), suggesting that in such steps the amine groups closest to the pyrazole ring are the ones protonating at a larger extent.

The changes with pH of the ^{13}C NMR labeled as C5 and C9 (see Figure 1b) support also the major participation of the nitrogen atoms closest to the pyrazole ring at this stage. While C5, which is placed in β-position with respect to amine groups N1 and N2,[26] experiences a continuous upfield shift upon protonation of **L1**, C9, which is just placed in β-position with respect to N2, only moves significantly upfield in correspondence with the first and third protonation steps of **L1**.

Pyridinophane **L2** has comparable basicity to **L1** in its first protonation and lower basicity in the following three next steps. In agreement with what has been observed for related pyridine macrocycles,[27,28] protonation of the pyridine is not observed in the 2−11 pH range in which the potentiometric measurements were carried out. As shown in Supporting Information Figure S2, the largest hypochromicity and hypsochromic shifts in the UV spectra are observed from pH 9 to 5, suggesting that, in this case, the second and third protonation steps are mostly affecting the secondary nitrogen atoms closest to the pyridine spacer.

Cu^{2+} Coordination. *Crystal Structure of $[Cu_2(H(H_{-1}L1))(H_{-1}L1)](ClO_4)_3\cdot 3.75H_2O$ (1).* Crystals of $[Cu_2(H(H_{-1}L1))(H_{-1}L1)](ClO_4)_3\cdot 3.75H_2O$ (**1**) were grown by slow evaporation of aqueous solutions containing **L1**·4HBr·H_2O and $Cu(ClO_4)_2\cdot 6H_2O$ in 1:1 mol ratio at pH 9. The crystral structure of **1** consists of $[Cu_2(H(H_{-1}L1))(H_{-1}L1)]^{3+}$ dinuclear dimeric cations, ClO_4^- anions, and lattice water molecules. Table 2 collects selected bond distances and angles,

Table 2. Selected Bond Distances (Å) and Angles (deg) for $[Cu_2(H(H_{-1}L1))(H_{-1}L1)](ClO_4)_3\cdot 3.75H_2O$ (1)

bond distance (Å)			bond angle (deg)			
Cu1	N12	1.955(3)	N12	Cu1	N6	93.84(14)
Cu1	N6	1.955(4)	N12	Cu1	N7	79.12(14)
Cu1	N7	2.070(4)	N6	Cu1	N7	165.43(15)
Cu1	N1	2.136(4)	N12	Cu1	N1	142.67(15)
Cu1	N8	2.221(4)	N6	Cu1	N1	80.21(15)
Cu2	N5	1.956(4)	N7	Cu1	N1	97.59(16)
Cu2	N11	1.965(3)	N12	Cu1	N8	113.78(15)
Cu2	N10	2.054(4)	N6	Cu1	N8	96.98(15)
Cu2	N4	2.163(4)	N7	Cu1	N8	97.53(15)
Cu2	N9	2.202(4)	N1	Cu1	N8	103.53(14)
			N5	Cu2	N11	94.18(14)
			N5	Cu2	N10	166.25(16)
			N11	Cu2	N10	78.90(14)
			N5	Cu2	N4	79.88(15)
			N11	Cu2	N4	140.10(17)
			N10	Cu2	N4	97.73(16)
			N5	Cu2	N9	95.27(15)
			N11	Cu2	N9	117.06(15)
			N10	Cu2	N9	98.46(15)
			N4	Cu2	N9	102.80(16)

and Supporting Information Table S1 details of the crystal structure refinement. In the dimeric $[Cu_2(H(H_{-1}L1))(H_{-1}L1)]^{3+}$ complex units the metal ions are connecting two different **L1** macrocycles (Figure 2a,b). In both macrocycles the pyrazole units are deprotonated behaving as bis(monodentate) ligands. Unlike most of the previously reported pyrazole azamacrocycles resulting from [2 + 2] and [3 + 2] condensations in which the pyrazolate units adopted an inner orientation to bind the metal ions,[18,30] in the present [1 + 1] macrocycle the pyrazolate anion displays an outer orientation which permits the binding of the metal ions in cooperation with a second macrocycle. As above-mentioned, a somewhat similar case was observed in the formation of the metallocage Cu^{2+} tetranuclear complex reported in ref 21.

The metal ions in **1** make a sort of hinge between the macrocycles which dispose the central parts of their polyamine chains toward opposite sides of the plane defined by the metal ions and the pyrazole units (Figure 2b). The Cu^{2+} metal ions

dx.doi.org/10.1021/ic400645t | Inorg. Chem. 2013, 52, 10795−10803

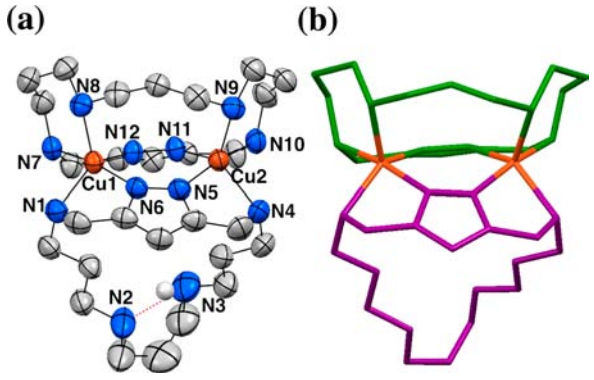

Figure 2. (a) View of the dinuclear dimeric complex $[Cu_2(H(H_{-1}\mathbf{L1}))(H_{-1}\mathbf{L1})]^{3+}$ of **1**. Ellipsoids are shown at 50% probability level. Hydrogen atoms omitted except the one of the ammonium group involved in intramolecular hydrogen bonding. (b) Two-colored view of the complex $[Cu_2(H(H_{-1}\mathbf{L1}))(H_{-1}\mathbf{L1})]^{3+}$ of **1** highlighting the connection between the macrocycles.

have in both sites distorted square pyramidal geometry with strong trigonal bipyramidal component (τ = 0.38 and τ = 0.43 for Cu1 and Cu2, respectively).[29] The equatorial plane is defined by two nitrogen atoms belonging to pyrazolate fragments of different macrocycles and by two contiguous secondary nitrogen atoms, also of different macrocycles. The elevation of both Cu^{2+} ions above the mean plane defined by the equatorial nitrogen atoms is ca. 0.46 Å. The distance between the copper atoms (3.9496(8) Å) is fixed by the nature of the pyrazolate bridges and is close to that usually observed in Cu^{2+} complexes of [2 + 2] pyrazole macrocycles with a similar bridging scheme.[18,30] The axial positions are occupied by two amine groups at the central part of the polyamine chain, but in this case belonging to the same macrocyclic unit (Figure 2a).

The equivalent amine groups of the other macrocycle remain uncoordinated, one of them being protonated at the pH values where these crystals evolved (Figure 2). Formation of an intramolecular hydrogen bond between the protonated (N3) and nonprotonated (N2) amine groups of this noncoordinating bridge portion is also observed. The N2−N3 distance is 2.661(9) Å. This pattern extends intermolecularly to connect the complexes through a relay of hydrogen bonds involving the protonated amine group, water molecules, perchlorate anions, and a coordinated amine group (see Supporting Information Figure S3). Hydrogen bonding contacts are collected in Supporting Information Table S2.

Crystal Structure of $[Cu_2(H(H_{-1}\mathbf{L1}))_{0.5}(H_{-1}\mathbf{L1})_{1.5}]_2(ClO_4)_3Br_2\cdot 4.2H_2O$ (**2**). When slowly evaporating solutions of $Cu(ClO_4)_2\cdot 6H_2O$ and **L1**·4HBr·H_2O at pH 10, crystals of $[Cu_2(H(H_{-1}\mathbf{L1}))_{0.5}(H_{-1}\mathbf{L1})_{1.5}]_2(ClO_4)_3Br_2\cdot 4.2H_2O$ (**2**) appeared. Details of the data collection, selected bond distances, and hydrogen bonding contacts are included in the Supporting Information (Tables S1, S3, and S4). All the bond distances and angles in the coordination sphere of the metal ions are close to those found in **1** (Figure 3 and Table S3). In this case, there are two bromide anions and three perchlorate anions shared by two dimeric complexes. One perchlorate is disordered in two possible positions. The main difference with respect to the previously discussed structure is that only one out of every four ligands has a protonated amine group in the noncoordinated chain. This part of the chain is disordered being observed two arrangements for the C4N2C5C6C7 set of atoms.

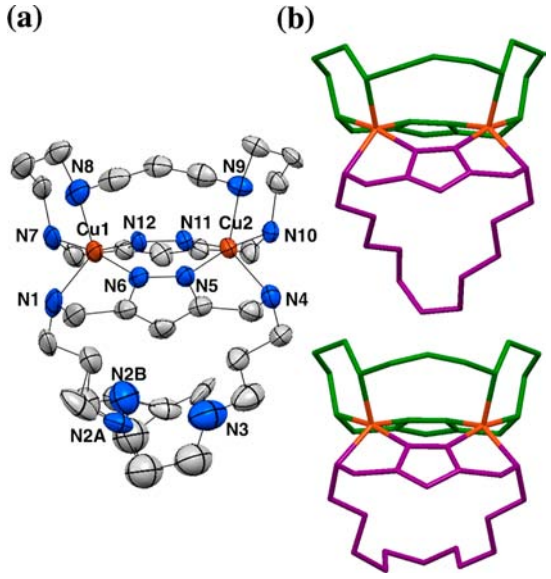

Figure 3. (a) ORTEP view of **2**.Counter ions are not shown. Ellipsoids are shown at 50% probability level. (b) Stick plots highlighting the two different dispositions of the noncoordinated lateral chain in the $[Cu_2(H(H_{-1}\mathbf{L1}))_{0.5}(H_{-1}\mathbf{L1})_{1.5}]^{2.5+}$ cation.

Crystal Structure of $[Cu\mathbf{L2}_2](ClO_4)_2$ (**3**). Compound **3** is formed by $[Cu\mathbf{L2}]^{2+}$ monomeric cationic complexes and perchlorate counteranions. The crystal structure shows that Cu^{2+} is coordinated in a regular square pyramidal geometry (τ = 0.036). The pyridine nitrogen (N1), the two nitrogen atoms closest to the aromatic spacer (N2 and N5), and one of the nitrogen atoms (N3) of the central part of the chain surrounded by six-membered chelate rings conform the equatorial plane. The slightly distorted axial position is occupied by the remaining nitrogen atom (N4) (Figure 4).

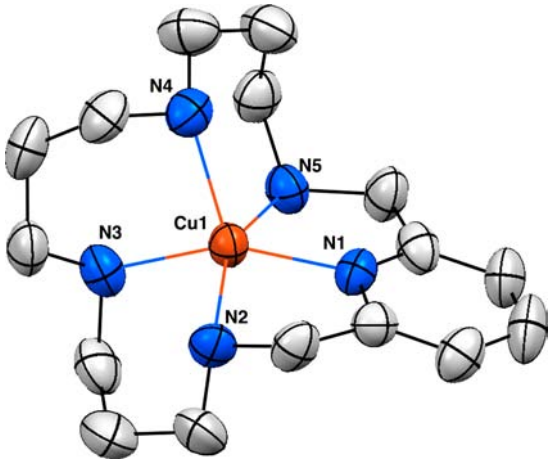

Figure 4. Molecular structure showing the cationic complex $[Cu\mathbf{L2}]^{2+}$. Ellipsoids are shown at the 50% probability level. Hydrogen atoms omitted.

Table 3 collects selected bond distances and angles. The shortest bond distance in the equatorial plane is that with the pyridine nitrogen, while the longest one is that with one of the contiguous secondary nitrogen atoms (N5), which is sharing the corner between five-membered and six-membered chelate rings. The location of this longest equatorial bond distance can be attributed to the aromatic spacer that prevents a closer

Table 3. Selected Bond Distances (Å) and Angles (deg) of Complex 3

bond distance (Å)			bond angle (deg)			
Cu1	N1	1.971(6)	N1	Cu1	N3	155.5(3)
Cu1	N3	2.028(5)	N1	Cu1	N2	80.6(3)
Cu1	N2	2.087(7)	N3	Cu1	N2	89.4(3)
Cu1	N5	2.125(6)	N1	Cu1	N5	80.5(3)
Cu1	N4	2.214(6)	N3	Cu1	N5	100.2(2)
			N2	Cu1	N5	153.3(3)
			N1	Cu1	N4	111.6(2)
			N3	Cu1	N4	92.8(2)
			N2	Cu1	N4	110.1(2)
			N5	Cu1	N4	94.4(2)

approach. The elevation of the copper atom above the nitrogen atoms in the equatorial plane is 0.41 Å. Unlike compound **1**, in this case only a few weak intermolecular hydrogen bonds have been observed (Table S5).

Crystal Structure of $[Cu_3(H_{-1}\mathbf{L1})_2(CO_3)(H_2O)](ClO_4)_2\cdot 8H_2O$ *(4).* Slow evaporation at pH 8 of aqueous solutions containing **L1**·4HBr·H_2O and $Cu(ClO_4)_2\cdot 6H_2O$ in 3:2 molar ratio led to the formation of crystals of $[Cu_3(H_{-1}\mathbf{L1})_2(CO_3)(H_2O)](ClO_4)_2\cdot 8H_2O$ (**4**) composition suitable for X-ray diffraction analysis. The structure reproduces the essential features of **1** and **2** with two macrocycles connected by two Cu^{2+} metal ions, but it has an additional Cu^{2+} bound to the two amine groups that remained free in one of the bridges of **1** or **2** (Figure 5a,b). Interestingly, this third Cu^{2+} completes its equatorial plane with a carbonate anion bound in a η^1,η^2-bidentate fashion with an O−Cu−O angle of 66.2(2)° (selected bond distances, angles, and hydrogen bonding contacts are collected in Table 4 and in Supporting Information Tables S6 and S7). The axial position

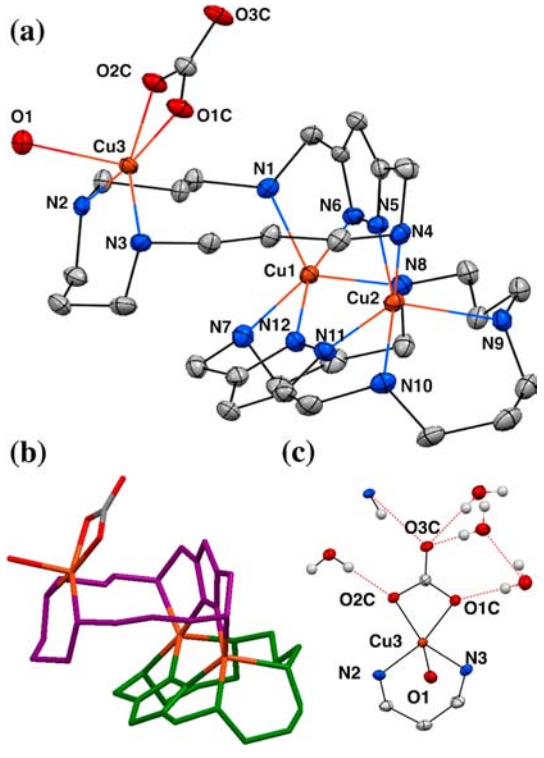

Figure 5. (a) ORTEP plot of the $[Cu_3(H_{-1}\mathbf{L1})_2(CO_3)(H_2O)]^{2+}$. Ellipsoids are shown at the 50% probability level. Hydrogen atoms omitted. (b) View highlighting with different colors the two macrocycles present in **4**. (c) View of the carbonate binding site and hydrogen bonding network.

Table 4. Selected Bond Distances (Å) and Angles (deg) of Cu3 Coordination Site in 4

bond distance (Å)			bond angle (deg)			
Cu3	O1C	1.988(3)	O1C	Cu3	O2C	66.17(12)
Cu3	O2C	1.998(3)	O2C	Cu3	N2	98.94(13)
Cu3	N2	1.999(3)	O1C	Cu3	N3	93.94(13)
Cu3	N3	2.023(3)	N2	Cu3	N3	100.26(14)
Cu3	O1	2.315(3)	O1C	Cu3	O1	92.72(12)
			O2C	Cu3	O1	101.85(12)
			N2	Cu3	O1	91.52(12)
			N3	Cu3	O1	91.38(13)

of the square pyramid (τ = 0.15) is occupied by a water molecule. The narrow angle imposed by the carbonate ligand provides a rather rhombic geometry to the system as evidenced by the EPR spectra of the crystals (see Figure S4). Since carbonate or carbon dioxide was not introduced as a reactant in the reaction flask, CO_2 should have been fixed from the atmosphere. Carbonate fixation is reinforced in the solid state by an extensive hydrogen bond network; while the coordinated oxygen atoms O1C and O2C hydrogen bond to a lattice water molecule and to the coordinated water molecule of another complex, O3C forms a trifurcated hydrogen bond with an amine group and two lattice water molecules (Figure 5c).

Such a CO_2 fixation induced by an unsaturated Cu^{2+} coordination site forming part of a larger preorganized complex entity puts into evidence one of the potential application of the ligand **L1** reported in this work.

Cu^{2+} Complex Formation in Solution. The stability constants for the systems Cu^{2+}−**L1** and Cu^{2+}−**L2** determined in 0.15 mol dm^{-3} $NaClO_4$ at 298.1 K have been included in Table 5, and the distribution diagrams in Figure 6 and

Table 5. Stability Constants for the Systems Cu^{2+}−L1 and Cu^{2+}−L2[a]

reaction[b]	L1	L2
$Cu + 2H + L \leftrightarrows CuH_2L$	26.76(1)[c]	26.88(8)
$Cu + H + L \leftrightarrows CuHL$		23.29(7)
$Cu + L \leftrightarrows CuL$		20.08(1)
$2Cu + H + 2L \leftrightarrows Cu_2HL_2$	43.00(1)	
$2Cu + 2L \leftrightarrows Cu_2L_2$	37.491(8)	
$2Cu + 2L \leftrightarrows Cu_2H_{-1}L_2 + H$	29.81(2)	
$2Cu + 2L \leftrightarrows Cu_2H_{-2}L_2 + 2H$	20.23(5)	
$3Cu + 2L \leftrightarrows Cu_3H_{-2}L_2 + 2H$	27.92(2)	
$3Cu + 2L \leftrightarrows Cu_3H_{-2}L_2(OH) + 3H$	20.20(4)	

[a]Logarithms of the constants are reported. [b]Charges omitted. [c]Values in parentheses are standard deviations in the last significant figure.

Supporting Information Tables S5 and S6. In order to select the best speciation model, particularly for the system Cu^{2+}:**L1**, different titrations were carried out varying not only the Cu^{2+}:**L1** molar ratio but also the concentration of the ligand and metal ion. The speciation study shows in both systems for 1:1 Cu^{2+}:**L** molar ratios the formation of complexes of 1:1 Cu^{2+}:**L** stoichiometry. However, as the X-ray studies evidenced the formation of 2:2 Cu^{2+}:**L1** dimeric dinuclear complexes, we carried out ESI mass spectrometry and EPR measurements to ascertain the nature of the complexes formed at the

dx.doi.org/10.1021/ic400645t | Inorg. Chem. 2013, 52, 10795−10803

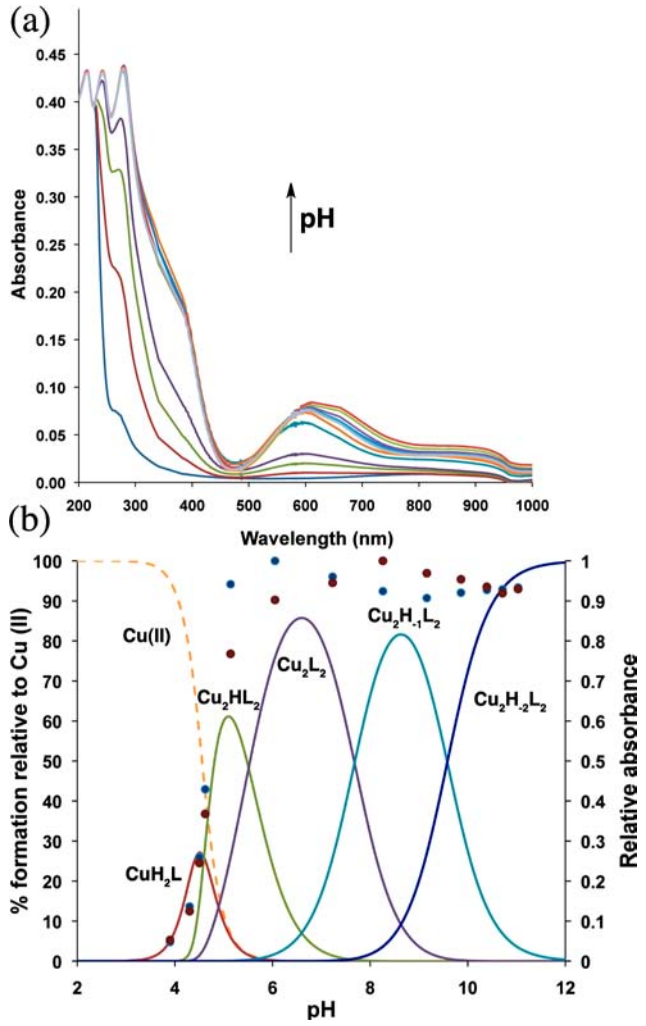

Figure 6. (a) UV−vis spectra of aqueous solutions containing Cu^{2+}:**L1** in 1:1 molar ratio recorded as a function of pH (pH values: 3.9, 4.3, 4.5, 4.6, 5.1, 6.0, 7.2, 8.2, 9.2, 9.9, 10.4, 10.7, and 11.0). (b) Plot of the distribution diagram of the system Cu^{2+}:**L1** for 1:1 molar ratio ($[Cu^{2+}] = 1 \times 10^{-3}$ M, I = 0.15 mol dm^{-3} $NaClO_4$, T = 298.1 ± 0.1 K, charges omitted) along with the absorbance values at 376 (blue) and 600 nm (red). Absorbances are normalized with respect to the maximum values at each wavelength.

concentration range used in the titrations (ca. 10^{-4}−10^{-3} M). HR-ESI-MS spectra recorded in the positive mode of aqueous solutions containing $Cu(ClO_4)_2 \cdot 6\ H_2O$ and **L1**·4HBr·H_2O adjusted to pH 7 and 9 show basically the existence in solution of dimeric dinuclear 2:2 species as denoted by the m/z peaks at 342.1597, 719.2853, 783.2653, and 795.2643 which correspond to the species $[Cu_2(H_{-1}\mathbf{L1})_2]^{2+}$, $[Cu_2(H_{-1}\mathbf{L1})_2(Cl)]^{+}$, $[Cu_2(H_{-1}\mathbf{L1})_2(ClO_4)]^{+}$, and $[Cu_2(H_{-1}\mathbf{L1})_2(CH_3OH)(Br)]^{+}$, respectively (see Figure S7). A very good agreement between the experimental and simulated isotopic distributions was obtained in all the cases.

Moreover, in the EPR spectra of solutions containing Cu^{2+} and **L1** recorded at pH values 2.3, 3.8, 5.5, 7.5, 9.5, and 11, it can be seen that while at pH values 2.3 and 3.8 the signal of free aqueous Cu^{2+} ion appears, the other solutions are EPR silent (see Supporting Information Figure S8). Taking into account the magnetic susceptibility study and previous reports on pyrazolate bridged complexes,[31] this can be ascribed to the formation of dinuclear complexes with a strong antiferromagnetic coupling occurring through the pyrazolate bridges (see below). Therefore, these experiments suggest that the stoichiometry of the species existing in equilibrium above pH 5 should be 2:2 instead of 1:1. This is also supported by the fitting of the pH-metric titrations. This means that, as it happened in the solid state, also in solution the pyrazolate subunits have to be disposed outward from the macrocyclic cavity, which makes a clear-cut difference with **L2** containing a pyridine ring or with other ligands containing pyrazole units.[32] The analysis of the UV−vis spectra agrees with the formation of only one type of complexes at this molar ratio. As early as the dinuclear $[Cu_2(\mathbf{L1})_2]^{4+}$ species starts forming in solution (pH ca. 4, Figure 6a), the intensity of the peaks at 376 and 600 nm increases reaching a maximum at pH 6 accordingly with the full formation of the dinuclear species. Since then on, dimeric dinuclear species prevail throughout all the pH range, and no further changes in the UV−vis spectra are observed (Figure 6b).

When speciation studies were performed for solutions with molar ratios Cu^{2+}:**L1** over 1, complexes of higher nuclearity needed to be introduced in the model to obtain a satisfactory fitting of the system. Although in principle a $[Cu_2(H_{-1}L)(OH)]^{2+}$ species could provide a reasonable fitting, the HR-ESI mass and EPR spectra and the previously discussed crystal structure **4** did not support this stoichiometry. EPR spectra showed the presence of a paramagnetic mononuclear Cu^{2+} center (Figure S4) while the HR-ESI mass spectra of solutions presented a peak at 408.5914 that could be ascribed to the species $[Cu_3(H_{-1}\mathbf{L1})_2Cl_2]^{2+}$ (Figure S9). Therefore, we introduced in our model species of this stoichiometry finding the best fit for the species $[Cu_3(H_{-1}\mathbf{L1})_2]^{4+}$ and $[Cu_3(H_{-1}\mathbf{L1})_2(OH)]^{3+}$ in agreement with the X-ray and mass spectra. It has to be emphasized that while distribution diagrams calculated for 1:1 Cu^{2+}:**L** molar ratio do not show formation of complexes of 3:2 Cu^{2+}:L stoichiometry, distribution diagrams calculated for 3:2 Cu^{2+}:**L** molar ratio show that such species predominate above pH 7 (Figure S5).

In order to estimate the stability of the ternary complexes we carried out titrations of solution containing Cu^{2+}, **L1**, and CO_3^{2-} in 3:2:3 molar ratios from basic to acidic pH values. Data obtained in the pH range 10.0−7.0 were treated with the HYPERQUAD program[33] giving a value of $\log \beta = 32.40(4)$ for the reaction $3Cu^{2+} + 2\mathbf{L1} + CO_3^{2-} \leftrightarrows [Cu_3(H_{-1}\mathbf{L1})_2(CO_3)]^{2+}$. The distribution diagram for this system (see Figure S10) provides evidence that the ternary complex predominates from pH 10.0 to 7.5, which indicates an important ability for fixing CO_2.

In the case of **L2**, the value obtained for the stability constant of the $[Cu\mathbf{L2}]^{2+}$ complex compares well with the stability values reported for the open-chain pentaamine 1,5,8,11,15-pentaazatetradecane ($\log K_{CuL} = 21.28$)[34] or with a related pyridinophane in which this polyamine subunit had been connected to a 2,6-pyridine spacer through methylene groups ($\log K_{CuL} = 20.44$),[32] suggesting that the pentacoordination observed in the crystal structure of **3** is also kept in solution.

Magnetic Behavior. The magnetic properties of **1** are shown in Figure 7 in the form of $\chi_M T$ versus T, χ_M being the magnetic susceptibility per two Cu^{2+} ions. The value of $\chi_M T$ at room temperature is 0.44 cm^3 mol^{-1} K, a value that is significantly lower than that expected for two uncoupled Cu^{2+} ions. When the sample has been cooled, $\chi_M T$ continuously decreases, vanishing at around 70 K. This magnetic behavior is

dx.doi.org/10.1021/ic400645t | Inorg. Chem. 2013, 52, 10795−10803

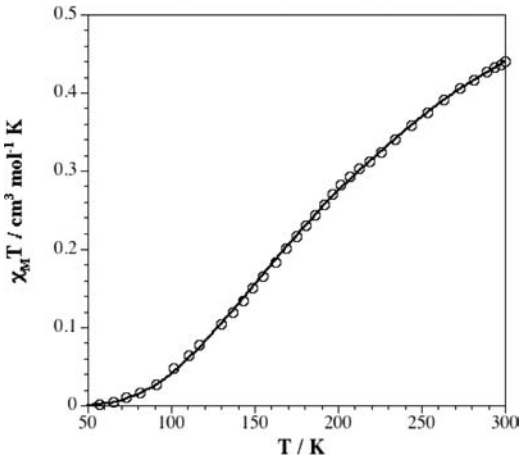

Figure 7. $\chi_M T$ vs T plot for compound **1**.

characteristic of an important antiferromagnetic interaction between the Cu^{2+} ions with singlet spin ground state.

Given that the interaction between dinuclear subunits is expected to be very weak, it is reasonable to assume that the magnetic properties are determined by the coupling within dinuclear subunits. For this reason we have interpreted the magnetic data according to the actual dinuclear nature of the complex through the spin Hamiltonian $H = -JS1S2$. The fit of the experimental data to the appropriate susceptibility expression derived from the van Vleck formula, and with the assumption that the g factors for both Cu^{2+} are identical, leads to $J = -299(5)$ cm^{-1} and $g = 2.06(1)$. The observed J values are within the range found for related bis(μ-pyrazolato)-bridged dinuclear complexes.[30,31]

The pathway for the magnetic exchange is propagated through the bridging pyrazolate moieties. From the molecular structure of **1**, one can conclude that the unpaired electron in each metal center is clearly described by a $d_{x^2-y^2}$ magnetic orbital which is coplanar with the pyrazolate skeleton. The significant overlap between these magnetic orbitals accounts for the strong antiferromagnetic coupling observed.

CONCLUSIONS

The synthesis of a [1 + 1] condensation pyrazole azamacrocycle is described. At least in the pH range 2−11, neither protonation nor deprotonation of the pyrazole unit is observed in this ligand. However, in the presence of an equivalent of Cu^{2+}, the pyrazole unit readily deprotonates to form 2:2 dimeric Cu^{2+} complexes with the pyrazolate moieties pointing outward hinging the two macrocyclic units. This makes an important difference with related cyclophanes containing pyridine spacers. The presence of the metal ions and free amine and ammonium groups within the same structural unit provides appealing characteristics for the recognition of guest species at this site of the molecule. As a matter of fact, we have shown that a third Cu^{2+} ion can be bound to the two free amine groups of the polyamines giving rise to an unsaturated coordination site which prompts this metalloreceptor for capturing further substrates. This is clearly demonstrated by the crystal structure of $[Cu_3(H_{-1}\mathbf{L1})_2(CO_3)(H_2O)](ClO_4)_2 \cdot 8H_2O$ (**4**) in which an atmospheric CO_2 molecule is efficiently fixed at this site. Future studies will be performed to address the possibility of using these complexes as catalysts in CO_2 chemistry.

EXPERIMENTAL SECTION

1*H*-3,5-Bis(chloromethyl)pyrazole and 3,5-bis-(chloromethyl)-1-(tetrahydropyran-2-yl)-pyrazole were prepared as described in refs 24 and 25.

1,5,9,13-Tetra-(*p*-tolylsulfonyl)-1,5,9,13-tetraazatridecane. *N*,*N*′-Bis(3-aminopropyl)-1,3-propanediamine (10.0 g, 53.1 mmol) was dissolved in 400 mL of THF, and K_2CO_3 (53.6 g, 387.7 mmol) in 100 mL of water was placed in a three-necked round-bottom flask provided with mechanical stirring. Then, a solution of *p*-tolylsulfonyl chloride (55.4 g, 290.8 mmol) in 100 mL of THF was dropwise added over 1 h. The solution was kept under stirring for one day, and the organic phase was separated and vacuum evaporated to dryness. The residue was suspended in ethanol and refluxed for two hours. Then, it was filtrated and washed exhaustively with ethanol (yield: 89%). Mp: 128−130 °C. ^{1}H NMR (300 MHz, $CDCl_3$): δ 7.73 (d, 4H, J = 8 Hz), 7.62 (d, 4H, J = 8 Hz), 7.32−7.26 (m, 8H), 5.39 (t, 2H, J = 6 Hz), 3.13 (t, 4H, J = 8 Hz), 3.08 (t, 4H, J = 8 Hz), 2.98 (td, 4H, J_1 = 8 Hz, J_2 = 6 Hz), 2.42 (s, 6H), 2.41 (s, 6H), 1.91−169 (m, 6H). ^{13}C NMR (300 MHz, $CDCl_3$): δ 143.8, 143.5, 136.9, 135.7, 130.0, 129.9, 127.3, 127.1, 47.5, 46.6, 40.3, 29.5, 28.7, 21.6.

1^1-Tetrahydropyran-2-yl-3,7,11,15-*p*-toluensulfonyl-1(3,5)-pyrazolacyclohexadecaphane. 1,5,9,13-Tetra-(*p*-tolylsulfonyl)-1,5,9,13-tetraazatridecane (2.65 g, 3.29 mmol) and K_2CO_3 (4.21 g, 32.9 mmol) were suspended in CH_3CN (250 mL). To this mixture, 3,5-bis-(chloromethyl)-1-(tetrahydropyran-2-yl)-1*H*-pyrazole (820 mg, 3.29 mmol) in 150 mL was added dropwise over 2 h. The suspension was refluxed for further 20 h and then filtered off. The solution was vacuum evaporated to dryness. Purification was achieved by column chromatography (silica gel, chloroform/acetone = 25/1) (yield: 34%). Mp: 78−80 °C. ^{1}H NMR (400 MHz, $CDCl_3$): δ 7.73−7.63 (m, 8H), 7.40−7.28 (m, 8H), 6.27 (s, 1H), 5.58 (dd, 1H, J_1 = 10 Hz, J_2 = 2), 4.40 (d, 1H, J = 15 Hz), 4.27 (d, 1H, J = 15 Hz), 4.12 (d, 1H, J = 7 Hz), 4.07 (d, 1H, J = 7 Hz), 3.92−3.83 (m, 1H), 3.78−3.68 (m, 1H), 3.23−2.84 (m, 12H), 2.47 (s, 3H), 2.43 (s, 3H), 2.42 (s, 3H), 2.41 (s, 3H), 2.39−2.37 (m, 2H), 1.88−1.42 (m, 10H). ^{13}C NMR (400 MHz, $CDCl_3$): δ 148.9, 144.3, 143.5, 138.5, 135.7, 134.6, 130.2, 129.9, 127.5, 127.4, 127.3, 100.1, 84.4, 68.4, 48.3, 48.2, 47.9, 47.8, 47.5, 30.1, 29.7, 29.6, 21.7. ESI-MS observed m/z 1003.44; calcd for $[M + Na]^+$ 1003.32.

3,7,11,15-Tetraaza-1(3,5)-pyrazolacyclohexadecaphane tetrahydrobromide (L1·4HBr·H$_2$O). 1^1-Tetrahydropyran-2-yl-3,7,11,15-*p*-toluensulfonyl-1(3,5)-pyrazolacyclohexadecaphane. (2.64 g, 2.69 mmol) and phenol (12.18 g, 129 mmol) were suspended in HBr−AcOH 33% (130 mL). The mixture was stirred at 90 °C for 24 h and then cooled. The resulting residue was filtered off and washed several times with dry ethanol to give the product **L1** as its pentahydrobromide salt (yield: 65%). Mp: 250−257 °C. ^{1}H NMR (400 MHz, D_2O): δ 6.84 (s, 1H), 4.42 (s, 4H), 3.23−3.17 (m, 12H), 2.15−2.07 (m, 6H). ^{13}C NMR (400 MHz, D_2O): δ 138.9, 109.9, 43.8, 43.5, 43.4, 22.0, 21.9. ESI-MS observed m/z 281.24 calcd for $[M + H]^+$ 281.24. Anal. Calcd for $C_{14}H_{28}N_6 \cdot 4HBr \cdot H_2O$: C, 27.18; H, 5.54; N, 13.59. Found: C, 27.0; H, 5.5; N, 13.6.

3,7,11,15-Tetraaza-3,7,11,15-*p*-toluensulfonyl-1-(2,6)-pyridinacyclohexadecaphane. 1,5,9,13-Tetra-(*p*-tolylsulfonyl)-1,5,9,13-tetraazatridecane (1.5 g, 1.86 mmol) and K_2CO_3 (2.57 g, 18.6 mmol) were suspended in CH_3CN (250 mL). To this mixture was added 2,6-bis(bromomethyl)pyridine (0.49 g, 1.86 mmol) in 150 mL CH_3CN dropwise over 2 h. The suspension was refluxed for further 20 h and then filtered off. The solution was vacuum evaporated to dryness and the residue suspended in refluxing ethanol. Then, it was filtrated to give a white solid (yield: 88%). Mp: 157−160 °C. ^{1}H NMR (400 MHz, $CDCl_3$): δ 7.73 (d, 4H, J = 8 Hz), 7.62 (d, 4H, J = 8 Hz), 7.42−7.28 (m, 11H), 4.19 (s, 4H), 3.18 (t, 4H, J = 7 Hz), 2.98 (t, 4H, J = 7 Hz), 2.83 (t, 4H, J = 7 Hz), 2.46 (s, 6H), 2.42 (s, 6H), 1.61 (quin, 4H, J = 7 Hz), 1.09 (quin, 2H, J = 7 Hz). ^{13}C NMR (400 MHz, $CDCl_3$): δ 144.1, 143.9, 138.3, 135.5, 130.3, 130.2, 127.6, 127.5, 54.4, 48.9, 48.8, 48.6, 30.4, 30.2, 21.5, 21.4.

3,7,11,15-Tetraaza-1-(2,6)-pyridinacyclohexadecaphane tetrahydrobromide (L2·4HBr·2H$_2$O). 3,7,11,15-Tetraaza-3,7,11,15-*p*-toluensulfonyl-1-(2,6)-pyridinecyclohexadecaphane (1.78 g, 2.96

dx.doi.org/10.1021/ic400645t | *Inorg. Chem.* 2013, 52, 10795−10803

mmol) and phenol (9.4 g, 99 mmol) were suspended in HBr−AcOH 33% (100 mL). The mixture was stirred at 90 °C for 24 h and then cooled. The resulting residue was filtered off and washed several times with dry ethanol to give the product as its tetrahydrobromide salt (yield: 65%), which decomposes at 250 °C. ^{1}H NMR (400 MHz, D_2O): δ 7.92 (t, 1H, J = 8 Hz), 7.47 (d, 2H, J = 8 Hz), 4.53 (s, 4H), 3.31−3.39 (m, 12H), 2.15−2.30 (m, 6H). ^{13}C NMR (400 MHz, D_2O): δ 150.2, 139.5, 122.9, 50.55, 44.4, 42.1, 41.9, 22.1, 19.3. ESI-MS observed m/z 292.2, calcd for $[M + H]^+$ 292.24; observed m/z 314.2, calcd for $[M - Na]^+$ 314.2. Anal. Calcd for $C_{16}H_{29}N_5 \cdot 4HBr \cdot 2H_2O$: C, 29.51; H, 5.73; N, 10.76. Found: C, 29.4; H, 5.7; N, 10.6.

*$[Cu_2(H(H_{-1}$**L1**$))(H_{-1}$**L1**$)](ClO_4)_3 \cdot 3.75H_2O$* (**1**). Crystals of **1** were grown by slow evaporation of aqueous solutions containing **L1**·4HBr·H_2O and $Cu(ClO_4)_2 \cdot 6H_2O$ in 1:1 mol ratio at pH 9 in an open vessel. After several days, blue crystals of **1** suitable for X-ray diffraction were obtained. Anal. Calcd for $C_{28}H_{62,5}Cl_3Cu_2N_{12}O_{15,75}$: C, 31.94; H, 5.98; N, 15.96. Found: C, 31.8; H, 6.1; N, 15.8.

*$[Cu_2(H(H_{-1}$**L1**$))_{0.5}(H_{-1}$**L1**$)_{1.5}]_2(ClO_4)_3Br_2 \cdot 4.2H_2O$* (**2**). Crystals of **2** were obtained as those of **1** but with pH of 10. Anal. Calcd for $C_{56}H_{117.4}Br_2Cl_3Cu_4N_{24}O_{16.2}$: C, 35.27; H, 6.20; N, 17.63. Found: C, 35.5; H, 6.2; N, 17.6.

*$[Cu$**L2**$](ClO_4)_2$* (**3**). Crystals of **3** were obtained by slow evaporation of an aqueous solution containing $Cu(ClO_4)_2 \cdot 6H_2O$ and **L2**·4HBr·$2H_2O$ at pH 8 with an excess of $NaClO_4$. Anal. Calcd for $C_{16}H_{29}Cl_2CuN_5O_8$: C, 34.70; H, 5.28; N, 12.64. Found: C, 34.9; H, 5.6; N, 12.7.

*$[Cu_3(H_{-1}$**L1**$)_2(CO_3)(H_2O)](ClO_4)_2 \cdot 8H_2O$* (**4**). Crystals of **4** were grown by slow evaporation of aqueous solutions containing **L1**·4HBr·H_2O and $Cu(ClO_4)_2 \cdot 6H_2O$ in 2:3 mol ratio at pH 9 in an open vessel. After several days, blue crystals of **1** suitable for X-ray diffraction were obtained. Anal. Calcd for $C_{29}H_{72}Cl_2Cu_3N_{12}O_{20}$: C, 29.75; H, 6.20; N, 14.35. Found: C, 29.8; H, 6.3; N, 14.3.

Electromotive Force Measurements. The potentiometric titrations were carried out at 298.1 ± 0.1 K using $NaClO_4$ 0.15 M as supporting electrolyte. The experimental procedure (buret, potentiometer, cell, stirrer, microcomputer, etc.) has been fully described elsewhere.[35] The acquisition of the emf data was performed with the computer program PASAT.[36] The reference electrode was a Crison 52 40 Ag/AgCl electrode in 0.5 M NaCl solution. A Wilhelm bridge filled with 0.5 M NaCl was used to separate the glass and the reference electrode. The glass electrode (Crison 52 50 Ag/AgCl) was calibrated as a hydrogen-ion concentration probe by titration of previously standardized amounts of HCl with CO_2-free NaOH solutions and determination of the equivalent point by Gran's method,[37] which gives the standard potential, $E^{o\prime}$, and the ionic product of water (pK_w = 13.73(1)).

The computer program HYPERQUAD[33] was used to fit the protonation and stability constants. Solutions containing the ligand salts with Cu^{2+}:**L** molar ratios varying from 2:1 to 1:2 were titrated with NaOH. In the case of the system Cu^{2+}−**L1** nine independent titrations with Cu^{2+} concentrations ranging from 2.0×10^{-4} M to 1.1×10^{-3} M with a total of 769 experimental data points were carried out. The different titration curves for each ligand were treated as separated curves without significant variations in the values of the stability constants. Finally, the sets of data were merged together and treated simultaneously to give the final stability constants. For estimating the constant for the formation of the carbonate complexes, two titrations of solutions containing Cu^{2+}, **L1**, and Na_2CO_3 in 3:2:3 molar ratio were performed from basic to acidic pH values. The constants for the protonation of **L1** and carbonate, for the formation of binary Cu^{2+}−**L1** complexes, were introduced as fixed parameters, and then the constants for the formation of ternary Cu^{2+}−**L1**−CO_3^{2-} complexes calculated. When more than one model fit the experimental data, the most reliable chemical model was chosen by performing F tests at the 0.05 confidence level.[38,39] More details on data treatment are included in the Supporting Information.

NMR Measurements. The ^{1}H and ^{13}C NMR spectra were recorded on Bruker Advance DPX 300 MHz and Bruker Advance DPX 400 MHz spectrometer operating at 299.95 and 399.95 MHz for ^{1}H and at 75.43 and 100.58 MHz for ^{13}C. *tert*-Butyl alcohol was used as a reference standard (δ = 1.24 ppm for ^{1}H and δ = 70.36 ppm for ^{13}C).[40] Adjustments to the desired pH were made using drops of DCl or NaOD solutions. The pD was calculated from the measured pH values using the correlation pH = pD − 0.4.[41]

X-ray Analysis. Single crystals of **1** and **4** were measured in an Oxford diffraction Supernova diffractometer using Mo Kα radiation (λ= 0.710 73 Å) at 293 and 120 K, respectively. Single crystals of **2** and **3** were measured in an Enraf Nonius Kappa CCD diffractometer using Mo Kα radiation at 293 and 120 K, respectively. Structures were solved by direct methods using SIR97[42] and refined by full-matrix least-squares on all F^2 using SHELXL97[43] with the WinGX suite.[44] The non-hydrogen atoms were refined anisotropically, and hydrogen atoms were placed in calculated positions and refined using a riding model. Table S1 summarizes crystal data and final refinement parameters. Hydrogen bonds have been analyzed with SHELXL97. Molecular drawings were produced with the MERCURY program.[45]

Magnetic Susceptibility Measurements. Magnetic susceptibility measurements on polycrystalline samples of compound $[Cu_2(H(H_{-1}$**L1**$))(H_{-1}$**L1**$)](ClO_4)_3 \cdot 3.75H_2O$ were carried out in the 1.9−300.0 K temperature range with a Quantum Design SQUID magnetometer under an applied magnetic field of 5000 G. The experimental data were corrected for the diamagnetic contributions of the constituent atoms and the sample holder as well as for the temperature-independent paramagnetism of the Cu^{2+} ion (60×10^{-6} cm^3 mol^{-1}).

Spectrometric Measurements. HR-ESI mass spectra of solutions (water/methanol 50/50 vol/vol) containing **L1** and $Cu(ClO_4)_2 \cdot 6H_2O$ in 1:1 and 2:3 molar ratio were acquired in the positive ion mode using a Triple TOF 5600 hybrid quadrupole time-of-flight (TOF) mass spectrometer. N_2 was used as a curtain and nebulizing gas. The experiments were performed at a voltage of 5300 V and GS1 and GS2 (35 psi) ion source gas at 723.15 K. The AB SCIEX Peak View software was used for the analysis of the data.

Spectroscopic Measurements. Spectra of the samples containing the ligand and the complexes in 1:1 and 2:3 molar ratio (1×10^{-3} M) were recorded with an Agilent 8453 spectrometer UV−vis spectra at 293.15 K.

Electron Paramagnetic Resonance Measurements. X-band EPR spectra (ν = 9.47 GHz) of the frozen-matrix aqueous solutions at 70 K and Q-band EPR spectra (ν = 34.03 GHz) of $[Cu_3(H_{-1}$**L1**$)_2(CO_3)(H_2O)](ClO_4)_2 \cdot 8H_2O$ at 9 K were recorded in nonsaturating conditions on a Bruker ER 200 D spectrometer equipped with a helium cryostat.

■ ASSOCIATED CONTENT

Ⓢ Supporting Information

CIF data, crystallographic data, distribution diagrams, UV−vis spectra, EPR spectra, ESI-mass spectra, and experimental details. This material is available free of charge via the Internet at http://pubs.acs.org.

■ AUTHOR INFORMATION

Corresponding Author

*E-mail: enrique.garcia-es@uv.es.

Notes

The authors declare no competing financial interest.

■ ACKNOWLEDGMENTS

Financial support by the Spanish MINECO, MECD, and FEDER funds of the E.U. (Projects CTQ2010-14892 and CONSOLIDER INGENIO 2010 CSD2010-00065) and Generalitat Valenciana (PROMETEO 2011/008) is gratefully acknowledged. The authors would like to thank Prof. K. Rissanen and G. de Munno for their help with the X-ray analysis. R.B. and J.P.-J. want to thank MECD and MINECO for their Ph.D. grants.

REFERENCES

(1) Elguero, J. *Pyrazoles* in *Comprehensive Heterocyclic Chemistry II, A Review of the Literature 1982−1995*; Katrizky, A. R., Rees, C. V., Scriven, E. F. V., Eds.; Pergamon: New York, 1997; Vol. 3, pp 1−75.
(2) Mukheerjee, R. *Coord. Chem. Rev.* **2000**, *203*, 151−258.
(3) Chaudhuri, P.; Kataev, V.; Büchner, B.; Klauss, H.; Kersting, B.; Meyer, F. *Coord. Chem. Rev.* **2009**, *253*, 2261−2285.
(4) Vlugt, J. I.; Demeshko, S.; Dechert, S.; Meyer, F. *Inorg. Chem.* **2008**, *47*, 1576−1585.
(5) Prokofieva, A.; Prikhod'ko, A.; Enyedy, E.; Farkas, E.; Maringgele, W.; Demeshko, S.; Dechert, S.; Meyer, F. *Inorg. Chem.* **2007**, *46*, 4298−4307.
(6) Eisenwiener, A.; Neuburger, M.; Kaden, T. *Dalton Trans.* **2007**, 218−233.
(7) Brooker, S.; Davidson, T. C.; Hay, S. J.; Kelly, R. J.; Kennepohl, D. K.; Plieger, P. G.; Moubaraki, B.; Murray, K. S.; Bill, E.; Bothe, E. *Coord. Chem. Rev.* **2001**, *216−217*, 3−30.
(8) (a) Weller, H.; Siegfried, L.; Neuburger, M.; Zehnder, M.; Kaden, T. A. *Helv. Chim. Acta* **1997**, *80*, 2315−2328. (b) Eisenwiener, A.; Neuburger, M.; Kaden, T. *Dalton Trans.* **2007**, 218−233.
(9) Brooker, S. *Eur. J. Inorg. Chem.* **2002**, 2535−2547.
(10) Brooker, S.; Davidson, T. C.; Hay, S. J.; Kelly, R. J.; Kennepohl, D. K.; Plieger, P. G.; Moubaraki, B.; Murray, K. S.; Bill, E.; Bothe, E. *Coord. Chem. Rev.* **2001**, *3*, 216−217.
(11) Kaim, W. *Coord. Chem.* **2002**, *230*, 127−139.
(12) Haasnoot, J. G. *Coord. Chem. Rev.* **2000**, *200*, 131−185.
(13) Klingele, M. H.; Brooker, S. *Coord. Chem. Rev.* **2003**, *241*, 119−132.
(14) Beckmann, U.; Brooker, S. *Coord. Chem. Rev.* **2003**, *245*, 17−29.
(15) Raper, E. S. *Coord. Chem. Rev.* **1994**, *129*, 91−156.
(16) (a) Kumar, M.; Arán, V. J.; Navarro, P. *Tetrahedron Lett.* **1993**, *34*, 3159−3162. (b) Kumar, M.; Arán, V. J.; Navarro, P.; Ramos-Gallardo, A.; Vegas, A. *Tetrahedron Lett.* **1994**, *35*, 5723−5726.
(17) Arán, V. J.; Kumar, M.; Molina, J.; Lamarque, L.; Navarro, P.; García-España, E.; Ramírez, J. A.; Luis, S. V.; Escuder, B. *J. Org. Chem.* **1999**, *64*, 6135−6146.
(18) Lamarque, L.; Navarro, P.; Miranda, C.; Arán, V. J.; Ochoa, C.; Escartí, F.; García-España, E.; Latorre, J.; Luis, S. V.; Miravet, J. F. *J. Am. Chem. Soc.* **2001**, *123*, 10560−10570.
(19) Miranda, C.; Escartí, F.; Lamarque, L.; Yunta, M. J. R.; Navarro, P.; García-España, E.; Latorre, J.; Jimeno, M. L. *J. Am. Chem. Soc.* **2004**, *126*, 823−833.
(20) Noble, A.; Olguí, J.; Clérac, R.; Brooker, S. *Inorg. Chem.* **2010**, *49*, 4560−4569.
(21) Escartí, F.; Miranda, C.; Lamarque, L.; Latorre, J.; García-España, E.; Kumar, M.; Arán, V. J.; Navarro, P. *Chem. Commun.* **2002**, 936−937.
(22) Dierck, I.; Herman, G. G.; Goeminne, A. M.; Van der Kelen, G. P. *Bull. Soc. Chim. Bel.* **1993**, *102*, 63−66.
(23) (a) Richman, J. E.; Atkins, T. J. *J. Am. Chem. Soc.* **1974**, *96*, 2268−2270. (b) Bencini, A.; Burguete, M. I.; Luis, S. V.; Miravet, J. F.; García-España, E.; Soriano, C. *J. Org. Chem.* **1993**, *58*, 4749−4753.
(24) Röder, J. C.; Meyer, F.; Pritzkow, H. *Organometallics* **2001**, 811−817.
(25) Iturrino, L.; Navarro, P.; Rodríguez-Franco, I.; Contreras, M.; Escario, J. A.; Martínez, A.; Del Rosario Pardo, M. *Eur. J. Med. Chem.* **1987**, *22*, 445−451.
(26) (a) Frassineti, C.; Ghelli, S.; Gans, P.; Sabatini, A.; Moruzzi, M. S.; Vacca, A. *Anal. Biochem.* **1995**, *231*, 374−382. (b) Frassineti, C.; Alderighi, L.; Gans, P.; Sabatini, A.; Vacca, A.; Ghelli, S. *Anal. Bioanal. Chem.* **2003**, *376*, 1041−1052. (c) Dagnall, S. P.; Hague, D. N.; McAdam, M. E.; Moreton, A. D. *J. Chem. Soc., Faraday Trans.* **1985**, *81*, 1483−1494. (d) Hague, D. N.; Moreton, A. D. *J. Chem. Soc., Perkin Trans 2* **1994**, *2*, 265−270.
(27) Fernandes, A. S.; Cabral, M. F.; Costa, J.; Castro, M.; Delgado, R. *J. Inorg. Biochem.* **2011**, *105*, 410−419.
(28) Díaz, P.; García Basallote, M.; Mañez, M. A.; García-España, E.; Gil, L.; Latorre, J.; Soriano, C.; Verdejo, B.; Luis, S. V. *Dalton Trans.* **2003**, 1186−1193.
(29) Addison, A. W.; Rao, T. N.; Reedijk, J.; van Rijn, J.; Verschoor, G. C. *J. Chem. Soc., Dalton Trans.* **1984**, *7*, 1349−1356.
(30) Miranda, C.; Escartí, F.; Lamarque, L.; García-España, E.; Navarro, P.; Latorre, J.; Lloret, F.; Jiménez, H. R.; Yunta, M. J. R. *Eur. J. Inorg. Chem.* **2005**, 189−208.
(31) (a) Hanot, V. P.; Robert, T. D.; Kolnaar, J.; Haasnoot, Reedijk, H. K.; Spek, L. *J. Chem. Soc., Dalton Trans.* **1996**, 4275−4281. (b) Teichgräber, J.; Leibeling, G.; Dechert, S.; Meyer, F. *Z. Anorg. Allg. Chem.* **2005**, *631*, 2613−2618. (c) Singh, A. K.; van der Vlugt, J. I.; Demeshko, S.; Dechert, S.; Meyer, F. *Eur. J. Inorg. Chem.* **2009**, 3431−3439.
(32) Díaz, P.; García Basallote, M.; Mañez, M. A.; García-España, E.; Gil, L.; Latorre, J.; Soriano, C.; Verdejo, B.; Luis, S. V. *Dalton Trans.* **2003**, 1186−1193.
(33) Gans, P.; Sabatini, A.; Vacca, A. *Talanta* **1996**, *43*, 1739−1753.
(34) Aguilar, J. A.; Diaz, P.; Escartí, F.; García-España, E.; Gil, L.; Soriano, C.; Verdejo, B. *Inorg. Chim. Acta* **2002**, *39*, 307−316.
(35) García-España, E.; Ballester, M. J.; Lloret, F.; Moratal, J. M.; Faus, J.; Bianchi, A. *J. Chem. Soc., Dalton Trans.* **1988**, 101−104.
(36) Fontanelli, M.; Micheloni, M. *Proceedings of the I Spanish-Italian Congress on Thermodynamics of Metal Complexes*; Diputación de Castellón, Castellón, Spain, 1990.
(37) (a) Gran, G. *Analyst* **1952**, *77*, 661−671. (b) Rossotti, F. J.; Rossoti, H. *J. Chem. Educ.* **1965**, *42*, 375−378.
(38) Hamilton, W. C. *Statistics in Physical Chemistry*; The Roland Press Co.: New York, 1964.
(39) Bologni, L.; Sabatini, A.; Vacca, A. *Inorg. Chim. Acta* **1983**, *69*, 71−75.
(40) Gottlieb, H. E.; Kotlyar, V.; Nudelman, A. *J. Org. Chem.* **1997**, *62*, 7512−7515.
(41) Covington, A. K.; Paabo, M.; Robinson, R. A.; Bates, R. G. *Anal. Chem.* **1968**, *40*, 700−706.
(42) Giacovazzo, C. *J. Appl. Crystallogr.* **1999**, *32*, 115−119.
(43) Sheldrick, G. M. *Acta Crystallogr., Sect. A* **2008**, *64*, 112−122.
(44) Farrugia, L. *J. Appl. Crystallogr.* **1999**, *32*, 837−838.
(45) Macrae, C. F.; Bruno, I. J.; Chisholm, J. A.; Edgington, P. R.; McCabe, P.; Pidcock, E.; Rodriguez-Monge, L.; Taylor, R.; van de Streek, J.; Wood, P. A. *J. Appl. Crystallogr.* **2008**, *41*, 466−470.